REPORT DOCUMENTATION PAGE

1. REPORT DATE (DD-MM-YYYY)	2. REPORT TYPE	3. DATES COVERED (From - To)
08-07-2008	Technical Paper	

4. TITLE AND SUBTITLE

Experimental and Computational Investigation of a RF Plasma Micro-Thruster (Preprint)

5a. CONTRACT NUMBER

5b. GRANT NUMBER

5c. PROGRAM ELEMENT NUMBER

6. AUTHOR(S)

J.D. Olliges (ERC); A.D. Ketsdever (AFRL/RZSA); W.B. Stein, A.A. Alexeenko, & I. Hrbud (Purdue University)

5d. PROJECT NUMBER

5e. TASK NUMBER

5f. WORK UNIT NUMBER
50260568

7. PERFORMING ORGANIZATION NAME(S) AND ADDRESS(ES)

Air Force Research Laboratory (AFMC)
AFRL/RZSA
10 E. Saturn Blvd.
Edwards AFB CA 93524-7680

8. PERFORMING ORGANIZATION REPORT NUMBER

AFRL-RZ-ED-TP-2008-284

9. SPONSORING / MONITORING AGENCY NAME(S) AND ADDRESS(ES)

Air Force Research Laboratory (AFMC)
AFRL/RZS
5 Pollux Drive
Edwards AFB CA 93524-7048

10. SPONSOR/MONITOR'S ACRONYM(S)

11. SPONSOR/MONITOR'S NUMBER(S)
AFRL-RZ-ED-TP-2008-284

12. DISTRIBUTION / AVAILABILITY STATEMENT

13. SUPPLEMENTARY NOTES

14. ABSTRACT

A prototype RF plasma micro-thruster has been investigated numerically and experimentally. The experimental results were obtained on a thrust stand capable of micro-Newton resolution. Thrust and mass flow (hence specific impulse) were measured for an argon propellant at mass flows ranging from 0.4 to 5.5 mg/sec. An increase to the cold gas thrust of up to 20% was observed for a discharge frequency of 100 MHz and an input power of 70 W. Propulsive efficiency was seen to increase both experimentally and numerically for increasing mass flow and decreasing discharge frequency.

15. SUBJECT TERMS

16. SECURITY CLASSIFICATION OF:			17. LIMITATION OF ABSTRACT	18. NUMBER OF PAGES	19a. NAME OF RESPONSIBLE PERSON
					Dr. Andrew Ketsdever
a. REPORT	b. ABSTRACT	c. THIS PAGE	SAR	9	19b. TELEPHONE NUMBER (include area code)
Unclassified	Unclassified	Unclassified			N/A

Experimental and Computational Investigation of a RF Plasma Micro-Thruster (Preprint)

J.D.Olliges[†], A.D. Ketsdever[‡],

[†] University of Southern California, Aerospace and Mechanical Engineering, Los Angeles, CA 90089
[‡] Air Force Research Laboratory, Edwards AFB, CA 93524

W.B. Stein, A.A. Alexeenko, and I. Hrbud

Purdue University, School of Aeronautical and Astronautical Engineering, West Lafayette, IN 47907

Abstract. A prototype RF plasma micro-thruster has been investigated numerically and experimentally. The experimental results were obtained on a thrust stand capable of micro-Newton resolution. Thrust and mass flow (hence specific impulse) were measured for an argon propellant at mass flows ranging from 0.4 to 5.5 mg/sec. An increase to the cold gas thrust of up to 20% was observed for a discharge frequency of 100 MHz and an input power of 70 W. Propulsive efficiency was seen to increase both experimentally and numerically for increasing mass flow and decreasing discharge frequency.

NOMENCLATURE

A_e = Area of the nozzle exit [m^2]
C = Effective exhaust velocity [m/s]
C_D = Coefficient of discharge
F = Thrust [N]
F_{CG} = Cold Gas thrust [N]
F_P = Powered thrust [N]
g_0 = Earth's gravitational constant [m/s^2]
I_{sp} = Specific impulse [s]
$\dot{m}$ = Mass flow rate [mg/s]
n_e = Electron number density [m^{-3}]
P_a = Ambient pressure [Pa]

P_e = Nozzle exit pressure [Pa]
P_{Jet} = Jet power [W]
P_{in} = Supplied electrical power [W]
r = Radius [m]
r_0 = Inner radius of discharge annulus [m]
r_1 = Outer radius of discharge annulus [m]
T_{gas} = Neutral gas temperature [K]
U_e = Nozzle exit velocity [m/s]
V = Applied electrode potential [V]
η = Thruster efficiency

INTRODUCTION

An increasing need for inexpensive, highly flexible spacecraft for scientific and industrial applications has fostered research into designing practical microsatellites (satellites having less than 100 kg of mass). Microsatellites have the prospect of replacing larger, more expensive spacecraft, either as solitary units or through multiple component formations, by utilizing a more adaptable, survivable platform.[1,2] The severe mass and power limitations imposed on small satellite designs imply that individual subsystems, including propulsion systems, need to be highly optimized.[1] Providing efficient means for station-keeping, attitude control, and mission-specific maneuvering on small-scale satellites is extremely challenging, and optimizing these propulsion systems to minimize mass and meet

power constraints while maintaining strict performance requirements becomes essential to the success of microsatellite systems.

One proposed concept for small spacecraft propulsion is the RF plasma thruster. Classified as an electrothermal propulsion system, this device uses a Radio-Frequency capacitively coupled discharge (RFCCD) to heat a propellant by creating a glow discharge plasma between two coaxial electrodes.[3] An electrothermal thruster is defined as one that uses electric power to heat a gas. Traditionally, this has involved a resistive heating element (resistojet)[4] or an arc (arcjet)[5] to heat the propellant. In the RF plasma thruster, the generated plasma is used as the heating element to heat the otherwise neutral gas flow. Propulsive performance relies on several macroscopic parameters including RF frequency (1 MHz to 1GHz) and power, propellant, mass flow rate, and geometry. These parameters will determine plasma formation and plasma characteristics, which will ultimately affect propellant heating and thruster lifetime.[6] Experimentally investigating the wide range of operating parameters required to optimize thruster performance is not practical. Experimental results obtained in this study were used to verify the results of a computational modeling effort which provides a cheaper, more viable alternative to experimental thruster optimization.

The RFCCD, shown schematically in Fig. 1, is a prototype device similar to that described in Ref. 3. The potential was applied to concentric electrodes via a coaxial (50-Ω impedance) feed from the RF power supply. The diameter ratio between the inner and outer electrodes produced a 50-Ω impedance to match that of the coaxial cables resulting in minimal power loss due to reflection. Propellant was fed to the thruster plenum through a showerhead arrangement of twelve orifices of 1.59mm diameter. The discharge was struck between the inner and outer electrodes in the plenum. For the proof-of-principle experiments described here, the gas was expanded through a 2.69mm diameter orifice. The RFCCD used in the experimental study is shown in Fig. 2.

To assess the thruster's propulsive capabilities the RF plasma thruster can be modeled numerically utilizing Particle-In-Cell/Monte Carlo Collision (PIC/MCC) and direct simulation Monte Carlo (DSMC) algorithms.[6,7] The PIC/MCC method is used to determine plasma characteristics within the coaxial discharge annulus. The argon collision model employed in the computations includes electron-neutral ionization, charge exchange, lumped excitation, and elastic scattering.[8] Neutral temperature variation within the discharge affects the plasma-neutral collision frequency and thus the power transmitted into the propellant. To account for heat transfer between the plasma and neutrals, a 1-D conduction model can be incorporated into the PIC simulation which utilizes power transmitted to the fluid via charge exchange and elastic collisions. This allows the plasma collisions and heating to vary with changes in neutral temperature. Thruster performance can be obtained using the DSMC method in conjunction with the neutral temperature predicted by the PIC/MCC simulation.
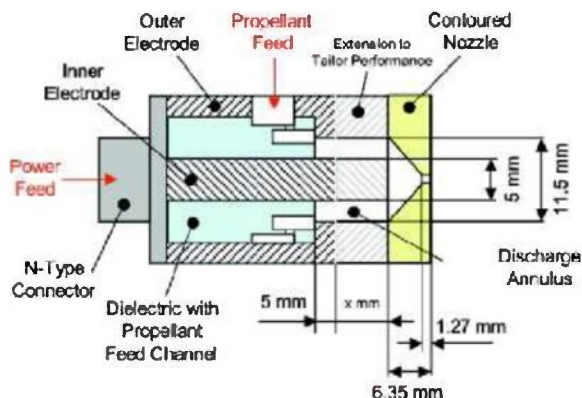
FIGURE 1. Schematic of the experimental RF plasma thruster.
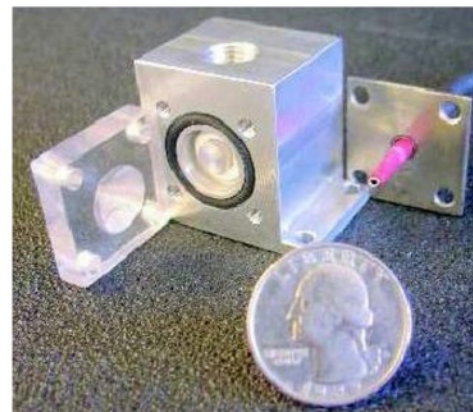
FIGURE 2. Experimental RFCCD.

Because of the strict weight and power requirements that microsatellites demand, successful micropropulsion systems require a rigorous optimization effort. Parametric optimization in the laboratory is expensive and time consuming, wherein a more cost-effective, practical option relies on numerical modeling to find optimal thruster operating conditions. Though numerical modeling provides a proficient method for thruster optimization, a macroscopic parameter verification is needed to verify the computational results. This paper experimentally addresses the RF plasma thruster's propulsive capabilities in order to substantiate the results obtained through PIC/MCC and DSMC modeling.

THEORY

Like most propulsive systems, the RF plasma thruster is designed to utilize propellant to create thrust. The thrust of a propulsion device is a measure of the force imparted by the expulsion of propellant (momentum thrust) and the force from the pressure differential across the nozzle exit plane (pressure thrust). Therefore, thrust is defined as

$$F = \dot{m}U_e + A_e \left(P_e - P_a \right) = \dot{m}C \tag{1}$$

where the momentum and pressure thrusts can be consolidated into a single term defined by an effective exhaust velocity. Propulsion systems are often characterized by their specific impulse, defined as

$$I_{sp} = \frac{F}{\dot{m}g_0} \tag{2}$$

The specific impulse is a measure of the amount of momentum transferred per unit mass of propellant. Generally, large I_{sp} indicates a propellant-efficient thruster. For electric thrusters, the propulsive efficiency is determined by the ratio of jet power (the power contained in the thruster plume) to the electrical power input into the system. P_{Jet} is defined by

$$P_{Jet} = \frac{1}{2}\dot{m}C^2 = \frac{1}{2}g_0 I_{sp}F \tag{3}$$

The thruster efficiency is then given by

$$\eta = \frac{P_{Jet}}{P_{in}} \tag{4}$$

NUMERICAL MODELING

The numerical method used to model the RF plasma thruster employed a combination of PIC/MCC[9] and DSMC algorithms. PIC/MCC was applied for kinetic plasma modeling to establish plasma characteristics within the thruster's discharge annulus. The charged test particles in the PIC/MCC calculations move in the electric field set up between the electrodes. Collisions between charged and neutral particles are calculated using the Monte Carlo method. The code used was XPDC1, a bounded, one dimensional simulation developed at the University of California at Berkeley by the Plasma Theory and Simulation Group. XPDC1, utilizing elastic scattering, lumped excitation, and electron-neutral ionization to model the power transfer to the propellant, was supplemented with a gas heat transfer (GHT) model to determine conductive heat-transfer due to plasma heating. Once the ion-neutral temperature was determined from PIC/MCC, DSMC simulations modeled the propellant expansion through the orifice and into the vacuum chamber. The PIC/MCC model inputs were pressure, voltage and frequency.

NUMERICAL RESULTS

Electron number density distributions for 0.5 and 2 Torr at 100 V for applied frequencies of 100, 130, and 160 MHz are compared in Fig. 3. These density distributions illustrate the transition from a diffusion dominated discharge at low pressures to a collisional asymmetric discharge at higher pressures. At lower pressures, electrons are able to traverse larger distances and diffuse through the gap between electrodes more easily. As a result the sheath width increases. A similar effect occurs when the applied frequency is decreased. This allows the electrons to travel in one direction longer per RF cycle and thus increases the sheath widths. The average and peak number densities increase with both discharge pressure and applied frequency and show trends previously shown by Lee et al.[10]
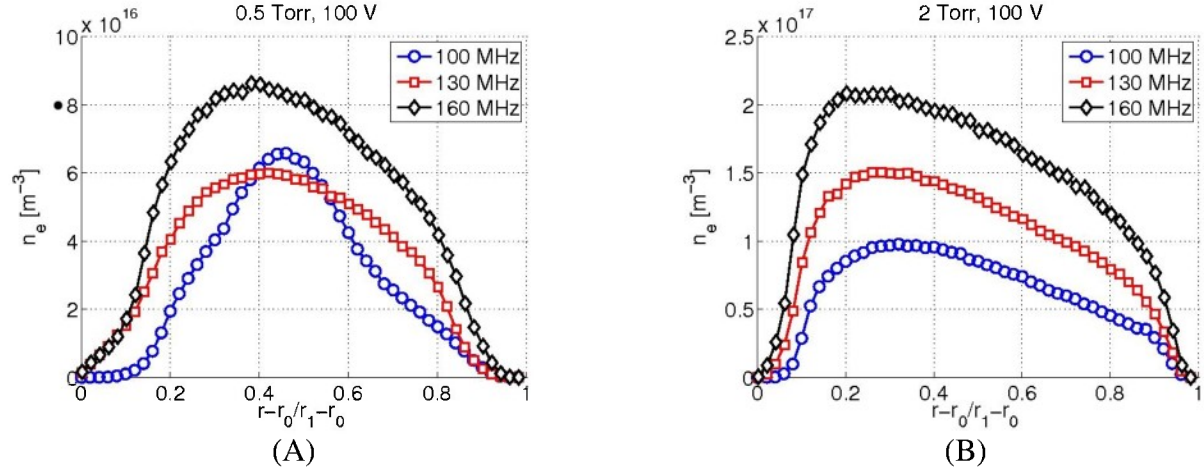
FIGURE 3: Calculated electron number density for V=100 Volts. (A) P_o=0.5 Torr, (B) P_o=2.0 Torr.
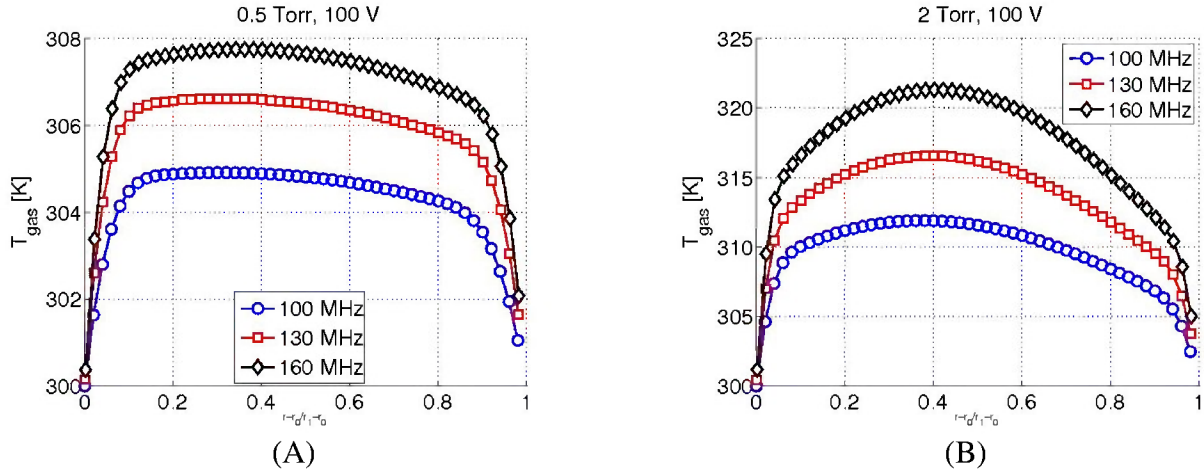
FIGURE 4: Calculated neutral gas temperature for V=100 Volts. (A) P_o=0.5 Torr, (B) P_o=2.0 Torr.

Figure 4 shows the comparison of calculated neutral gas temperature distributions for discharge pressures of 0.5 and 2 Torr and applied frequencies of 100, 130, and 160 MHz at 100 V. At a constant applied voltage, the neutral temperatures increase with increasing pressure and frequency. Higher pressure discharges have a higher ion-neutral charge exchange collision frequency which provides higher heating. This not only increases the neutral temperature of the discharge, but it also causes the discharge to have a more curved shape due to the increased heating in the sheaths. Increasing the applied frequency also increases the neutral temperature through increased power transmission into the fluid. Thus, increasing the applied frequency not only increases the neutral temperature but also decreases the discharge pressure if the mass flow rate through the thruster is held constant.

For electric thrusters, the measure of performance is the propulsive efficiency determined by Eqn. (4). The results of the PIC simulations can be used to assess the effects of frequency on the propulsive efficiency. Figure 5 shows the total power transmitted to the propellant as a function of pressure and frequency for a constant applied voltage. An increase in frequency must be offset by a decrease in either pressure or voltage to keep a constant applied power. As the applied voltage increases, the power transmitted into the propellant increases which causes a rise in the neutral gas temperature. Since the mass flow rate is held constant, the rise in gas temperature must come with an increase in pressure, causing the power transmission to increase until the discharge stabilizes. An increase in the applied frequency will act to decrease the applied potential since the pressure and temperature are constrained by the mass flow and cannot change for a constant power. Thus, for constant power, constant mass flow discharges, cases which operate at a higher frequency will operate at a reduced voltage compared to their lower frequency counterparts. This increase in applied frequency, and corresponding decrease in applied potential, reduces the transmission efficiency reducing the microthruster's performance.
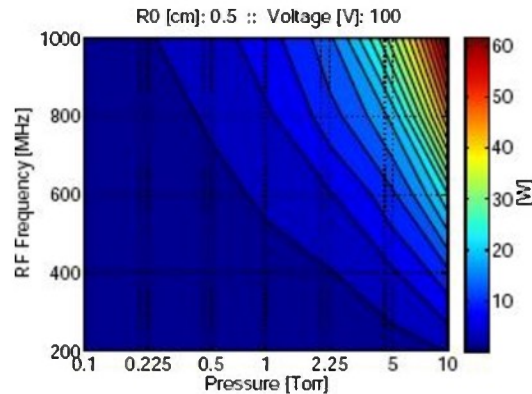
FIGURE 5. Power transmitted to propellant as a function of discharge pressure and applied frequency.

EXPERIMENTAL SETUP

The RF plasma thruster was tested inside the CHAFF-IV high vacuum chamber, a 6-m long, 3-m diameter stainless steel test chamber at the University of Southern California. CHAFF-IV is primarily pumped by a Zyrianka 900 diffusion pump capable of a 30,000 L/s pumping speed on nitrogen. The Zyrianka 900 provided background pressures of 10^{-5} to 10^{-4} Torr over the range of experimental thruster flow rates.

The thruster was attached to the arm of the nano-Newton thrust stand (nNTS) as shown in Fig. 6. The nNTS used in this study was a torsion thrust stand similar to that described by Jamison, et al.[11] Gas coupling was accomplished through a compression fitting-sealed, flexible rubber tube mounted along the rotational axis of the stand. RF power was attached through a 2.4-mm diameter, Kapton insulated coaxial cable secured above the stand and draped across the arm to minimize physical influence on the stand's movement. Thrust stand deflection was measured using a linear variable differential transformer (LVDT) attached to a 24-bit data acquisition card. An electrostatic comb calibration system, modified from the technique described by Selden and Ketsdever[12], was used for precise steady-state force calibration between 270 μN and 2.4 mN. The force curve provided by the electrostatic combs adequately spanned the range produced by the RF plasma thruster over the range of tested flow rates.

Gas flow to the thruster was measured with an Omega™ mass flowmeter. The flowmeter operates by creating a pressure differential in a laminar flow field. The flowmeter forces the gas into streamlined flow and measures the pressure drop across a known length of laminar flow. Measures of absolute temperature and pressure inside the meter correlate the volumetric flow rate to a standardized mass flow rate. Measurements correlating mass flow and line pressure were taken using a 1-Torr differential Baratron. Pressure measurements were obtained independently of thrust traces due to the complication of attaching the Baratron to the oscillating nNTS.

The RF power system consisted of a RF power amplifier and frequency generator. The RF power amplifier provided RF frequencies between 70 and 160 MHz at adjustable power levels between 0 and 100 W. The transmission line connecting the RF power system and thruster maintained 50-Ω impedance, thus minimizing power loss.

The total duration of a test sequence was 180 seconds and encompassed four 30-s segments and one 60-s segment. The first 30 seconds represents a "zero baseline" where neither gas nor power was supplied to the thruster. The second 30 seconds established a "cold gas baseline" where only gas was delivered to the thruster. After 60 seconds, power was supplied to the thruster, igniting the plasma that remained lit until the 90th second when the power supply was turned off. Gas was turned off after 120 seconds allowing the thrust stand to damp towards its zero baseline for the remainder of the test sequence. Figure 3 shows a typical trace and the displacements corresponding to the cold gas and powered thrust segments.

Powered thrust trials were taken for 100 Mhz, 130 Mhz, and 160 Mhz at 100 W forward power while mass flow to the thruster was varied between 0.4 and 5.5 mg/sec of Argon. P_{in} was considered the difference between forward power and reflected power where reflected power varied with mass flow and frequency. Additional tests with $\dot{m} =$ 1.225 ± 0.002 mg/sec and 160 Mhz frequency were taken with forward power levels of 30 W, 65 W, and 100 W to see the effects of varying power levels on thruster performance.
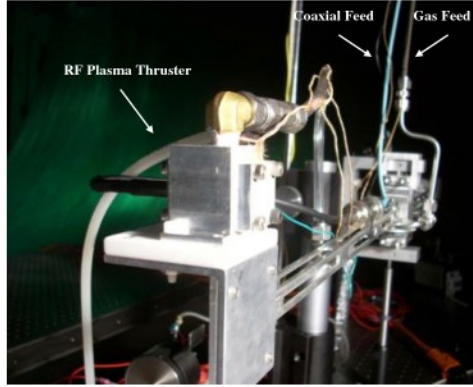
FIGURE 6. The RF Plasma thruster attached to the arm of the nNTS. The electrostatic comb calibration system was attached to the opposite arm of the thrust stand.

EXPERIMENTAL RESULTS

Several thruster performance characteristics were obtained experimentally in an effort to compare to numerical trends in order to verify the computational model. The ratio of RF powered thrust to unpowered (cold gas) thrust, F_P/F_{CG}, was measured to quantify the increase in thrust produced by igniting a plasma in the RFCCD. A typical powered thrust trace used to determine F_P/F_{CG} is shown in Fig. 7. For the nNTS trace shown in Fig. 7, the initial rise from zero is due to the initial unpowered gas flow to the thruster. Power was turned on at 60 seconds and allowed to remain on for the following 30 seconds. The slight increase in unpowered thrust when the power is turned off at 90 seconds is due to the heating of the thruster (and propellant) by the preceding powered operation. Figure 8 shows the thrust ratio, F_P/F_{CG}, for $\dot{m} = 1.225 \pm 0.002$ mg/sec and 160 MHz frequency as a function of input power levels. The magnitude of F_P/F_{CG} is directly related to the power input of the system. Operating the thruster at higher power levels increased thrust and decreased efficiency.
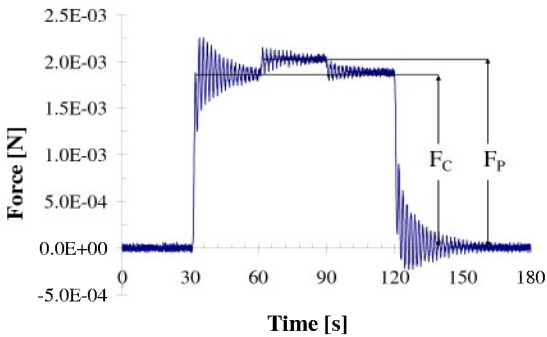
**FIGURE 7.** A typical powered trace from the nNTS.
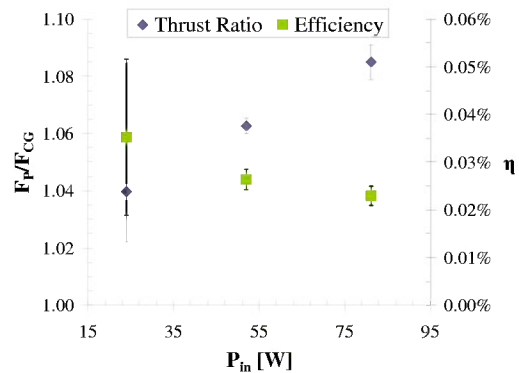
FIGURE 8. Thrust ratio and efficiency as a function of input power.

The thrust ratio was also examined as a function of frequency and mass flow as shown in Fig. 9. There are two potential mechanisms contributing to the shape of the thrust ratio plot. The first is the diminishing return of electron energy transfer as pressure in the chamber increases. At low pressures, there are few molecules in the discharge annulus, and the electrons within the plasma have few collisions each time the polarity of the electrodes swaps. Electrons gain speed in-between collisions, transfer large amounts of energy when they impact an argon atom, the gas temperature increases, and F_P/F_{CG} is large. As gas flow increases, the electrons collide with more argon atoms each time the polarity swaps and cannot get to the same speeds in-between collisions. Because the electrons do not transfer as much energy, the thrust ratio declines with increasing pressure.

The other determining factor in Fig. 9 is a plasma density based function. At low pressures, the power-coupling to the gas is inefficient resulting in a weak or diffuse plasma discharge. There are few free electrons

available to collide with Argon atoms yielding an overall low number of collisions. As pressure increases, the power transferred to the gas also increases, increasing plasma density. More free electrons allow more opportunities for atomic collisions. At the inflection point, the increase in plasma density begins to compensate for the diminishing energy transfer per collision. Though each collision is transferring smaller amounts of energy, the increased number of impacts begins to give the atoms more total energy allowing F_P/F_{CG} to increase.

The thruster's specific impulse for various discharge frequencies is shown as a function of mass flow rate in Fig. 10. The theoretical maximum cold gas specific impulse, shown as a straight line in Fig. 10, was computed using 1-D isentropic flow relationships assuming a discharge coefficient, $C_D = 1$. The experimental I_{sp} was several seconds less than the theoretical maximum due to viscous and other losses. Powered thrust measurements followed a trend similar to the thrust ratio in Fig. 9 and produced increases over cold gas specific impulse for all mass flows and frequencies. For mass flow rates above 1.25 mg/sec, powered I_{sp} increases with increasing mass flow. The increasing specific impulse signifies the thruster becomes more propellant efficient at larger mass flow rates and lower frequencies.
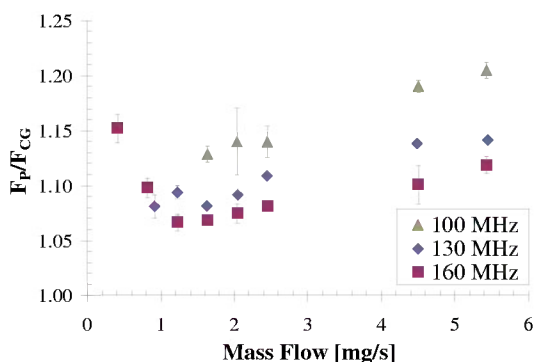
FIGURE 9. Thrust ratio as a function of $\dot{m}$ and frequency.
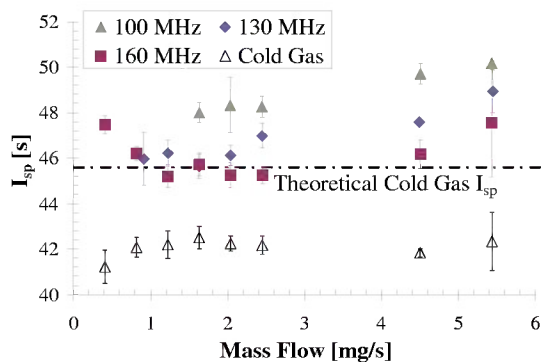
FIGURE 10. Specific impulse as a function of $\dot{m}$ and frequency.

Figure 11 shows how the RFCCD's propulsive efficiency varies with mass flow rate and frequency. As can be seen, the propulsive efficiency increases for increased mass flow. The efficiency also increases at a given mass flow rate for decreased discharge frequency. The input power used to calculate the propulsive efficiency in Fig. 11 was found by finding the difference in forward and reflected power. The jet power used was determined by taking the thrust and Isp difference between the powered and unpowered (cold gas) values. The values in Fig. 11 are low for a micropropulsion system; however, the thruster was not optimized in this study nor was it operated in the most efficient regime.

DISCUSSION

Cold gas experimental data of thrust versus mass flow validated the DSMC model used to evaluate the gas expansion through the exit orifice. Figure 12 shows experimental and numerical results for cold gas thrust using an argon propellant. Computational modeling produced cold gas thrust values within 8% of those obtained experimentally further validating the use of DSMC for orifice flows. Previous studies[13] have shown that DSMC accurately predicts cold gas thrust and specific impulse for rarefied and near-continuum flows. Errors in this study most likely stem from machining and measurement tolerances associated with the experimental orifice diameter, surface roughness, and the axi-symmetric nature of the DSMC simulations.

For powered thrust operation, the experiments were performed to give an adequate representation of the trends in thruster performance as a function of mass flow rate and frequency. These trends have been duplicated in the numerical modeling in several ways. First, the thrust produced by the RFCCD increased as a function of input power. Second, the propulsive efficiency increased with increasing mass flow. From Fig. 3, an increased mass flow for a constant power and frequency must lead to an increase in voltage. A voltage increase generally led to a higher transmission efficiency which gave a higher overall propulsive efficiency for the thruster. Figure 11 shows this same trend in the experimental results. Finally, the propulsive efficiency was higher for lower values of the discharge frequency. Again, Fig. 3 shows this trend for the numerical results, and Fig. 11 shows a similar trend observed experimentally. Geometry and operating parameters of the RFCCD will be optimized using future numerical results in an effort to increase thrust, specific impulse, and propulsive efficiency.
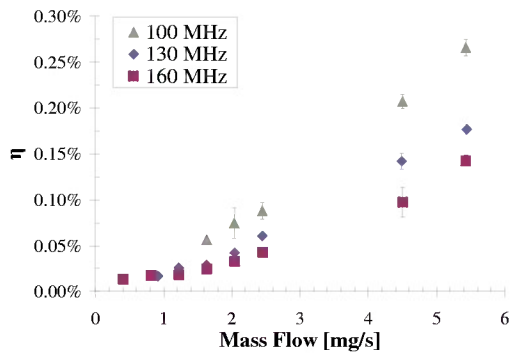
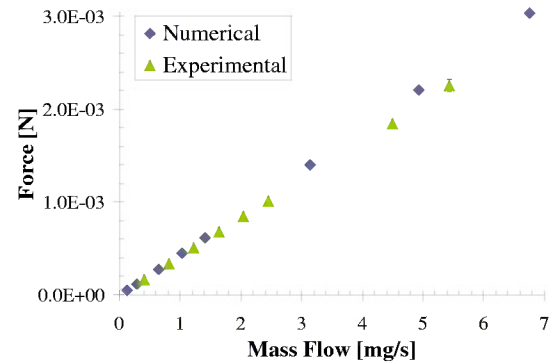**FIGURE 11.** Propulsive efficiency as a function of $\dot{m}$ and frequency.

FIGURE 12. Cold gas thrust as a function of $\dot{m}$.

ACKNOWLEDGMENTS

REFERENCES

1. M. M. Micci and A. D. Ketsdever, Micropropulsion for Small Spacecraft, USA: AIAA, 2000, pp. xvii,??
2. C. Sultan, S. Seereram, and R. K. Mehra, The International Journal of Robotics Research **26** 405-430 (2007).
3. I. Hrbud, G. E. Kemp, A. H. Yan, and J. G. Gedrimas, "Review of RF Plasma Thruster Development" in Proc. of the 30th International Electric Propulsion Conference, IEPC-2007-309, Florence, Italy, 2007.
4. A. D. Ketsdever, R. H. Lee and T. C. Lilly, J. Micromech. Microeng. **15** 2254-2263 (2005).
5. H. Horisawa, and I. Kimura, Vacuum. **59** 106-117 (2000).
6. W. B. Stein, A. A. Alexeenko and I. Hrbud, "Performance Modeling of an RF Coaxial Plasma Thruster" in Proc.of the 43rd Joint Propulsion Conference, AIAA Paper-2007-5292, Cincinnati, OH, 2007.
7. W. B. Stein, A. A. Alexennko and I. Hrbud, "RFCCD Microthruster Performance via Numerical Simulation" in Proc. of the 46th Aerospace Sciences Meeting, AIAA Paper-2008-962, Reno, NV, 2007.
8. J. E. Lawler and U. Kortshagen, J. Phy. D: Appl. Phys. **32** 3188-3198 (1999).
9. C. K. Birdsall. IEEE Transactions on Plasma Science. **19** 65-85 (1991).
10. J. K. Lee, N. Babaeva, H. C. Kim, O. Manuilenko, and J. W. Shon, Plasma Science **32** 47-53 (2004).
11. A. J. Jamison, A. D. Ketsdever and E. P. Muntz, Rev. Sci. Instrum. **73** 3629-3637 (2002).
12. N. P. Selden and A. D. Ketsdever, Rev. Sci. Instrum. **74** 5249-5254 (2003).
13. A. D. Ketsdever, M. T. Clabough, S. F. Gimelshein, and A. A. Alexeenko, AIAA J. **43** 633-641 (2005).